

System size dependence of intermediate mass fragments in heavy-ion collisions

Sukhjit Kaur

House No. 465, Sector-1B, Nasrali, Mandi Gobindgarh-147301, Punjab, India.

November 20, 2018

Electronic address: sukhjitk85@gmail.com

Abstract

We simulate the central reactions of $^{20}\text{Ne}+^{20}\text{Ne}$, $^{40}\text{Ar}+^{45}\text{Sc}$, $^{58}\text{Ni}+^{58}\text{Ni}$, $^{86}\text{Kr}+^{93}\text{Nb}$, $^{129}\text{Xe}+^{118}\text{Sn}$, $^{86}\text{Kr}+^{197}\text{Au}$ and $^{197}\text{Au}+^{197}\text{Au}$ at different incident energies for different equations of state (EOS), binary cross sections and different widths of Gaussians. A rise and fall behaviour of the multiplicity of intermediate mass fragments (IMFs) is observed. The system size dependence of peak center-of-mass energy $E_{c.m.}^{max}$ and peak IMF multiplicity $\langle N_{IMF} \rangle^{max}$ is also studied, where it is observed that $E_{c.m.}^{max}$ follows a linear behaviour and $\langle N_{IMF} \rangle^{max}$ shows a power law dependence. A comparison between two clusterization methods, the minimum spanning tree and the minimum spanning tree method with binding energy check

(MSTB) is also made. We find that MSTB method reduces the $\langle N_{IMF} \rangle^{max}$ especially in heavy systems. The power law dependence is also observed for fragments of different sizes at $E_{c.m.}^{max}$ and power law parameter τ is found to be close to unity in all cases except A^{max} .

1 Introduction

The behaviour of hot and dense nuclear matter at the extreme conditions of temperature and density is a question of keen interest. It can be studied with the help of heavy-ion reactions at intermediate energies. At high excitation energies, the colliding nuclei may break into several small and intermediate size fragments followed by a large number of nucleons [1–3]. A large number of experimental attempts had been carried out ranging from the evaporation of particles to the total disassembly of the dense matter. Besides these two extremes, one can also have a situation where excited matter breaks into several fragments. In the last few decades, several experimental groups have carried out a complete study of fragment formation with 4π detectors [4–10]. It is quite obvious from these studies that the fragments formed in heavy-ion collisions depend crucially on the bombarding energy and impact parameter of the reaction [1–5]. Therefore, these experimental studies of fragmentation offer a unique opportunity to explore the mechanism behind the formation of the fragments. Moreover, one can also pin down the role of dynamics in fragment formation and their time scale.

Recently, there has been increasing interest in the effects of reaction dynamics on the production of IMFs and light charged particles (LCPs, $Z=1$ or 2). Sisan *et al.* [6]

studied the emission of IMFs from central collisions of nearly symmetric systems using 4 π -Array set up where they found that the multiplicity of IMFs shows a rise and fall with increase in the beam energy. They observed that $E_{c.m.}^{max}$ (energy at which the maximum production of IMFs occurs) increases linearly with the system mass whereas a power law ($\propto A^\tau$) dependence was reported for peak multiplicity of IMFs with power factor $\tau = 0.7$. Peaslee *et al.* [7], on the other hand, studied asymmetric system $^{84}\text{Kr}+^{197}\text{Au}$ in the incident energy range from 35 to 400 MeV/nucleon and obtained an energy dependence of multifragmentation. Their findings revealed that fragment production increases up to 100 MeV/nucleon and then decreases with increase in incident energy. De Souza *et al.* [8] studied the central collisions of $^{36}\text{Ar}+^{197}\text{Au}$ from 35 to 120 MeV/nucleon and observed that IMF multiplicity shows a steady increase with increase in the incident energy. The IMF multiplicity decreases, however, when one moves from central to peripheral collisions. On the other hand, Tsang *et al.* [5], in their investigation of $^{197}\text{Au}+^{197}\text{Au}$ collisions at $E/A = 100, 250, \text{ and } 400$ MeV, found the occurrence of peak multiplicity at lower energies for central collisions whereas it is shifted to higher energies for peripheral collisions. Stone *et al.* [9] used a nearly symmetric system of $^{86}\text{Kr}+^{93}\text{Nb}$ from 35 to 95 MeV/nucleon to obtain IMF multiplicity distribution as a function of beam energy by selecting central events. Ogilvie *et al.* [10] also studied the multifragment decays of Au projectiles after collisions with C, Al, and Cu targets at the bombarding energy of 600 MeV/nucleon using ALADIN forward spectrometer at GSI, Darmstadt, with the beam accelerated by SIS synchrotron. They found that with increasing the violence of collision, the mean multiplicity of IMFs originating from projectile first increases to a maximum and then decreases again.

As mentioned earlier, Sisan *et al.* [6] reported that the peak multiplicity of IMFs as well as peak center-of-mass energy scale with the size of the system. In a recent communication, Vermani and Puri [11] succeeded partially in explaining the above mentioned behaviour by using the quantum molecular dynamics (QMD) approach. We here plan to extend the above study by incorporating various model ingredients such as equation of state, nucleon-nucleon (nn) cross section, and Gaussian width. The role of different clusterization algorithms shall also be explored. We shall attempt to find out whether these ingredients have sizable effects.

2 The Formalism

2.1 Quantum Molecular dynamics (QMD) model

We describe the time evolution of a heavy-ion reaction within the framework of Quantum Molecular Dynamics (QMD) model [1–3, 12] which is based on a molecular dynamics picture. The explicit two- and three-body interactions lead to the preservation of fluctuations and correlations that are important for N-body phenomena like multifragmentation. In QMD model each nucleon is represented by a Gaussian distribution whose centroid propagates with the classical equations of motion:

$$\frac{d\mathbf{r}_i}{dt} = \frac{dH}{d\mathbf{p}_i}, \quad (1)$$

$$\frac{d\mathbf{p}_i}{dt} = -\frac{dH}{d\mathbf{r}_i}, \quad (2)$$

where the Hamiltonian is given by

$$H = \sum_i \frac{\mathbf{p}_i^2}{2m_i} + V^{tot}, \quad (3)$$

with

$$V^{tot} = V^{loc} + V^{Coul} + V^{Yuk} + V^{MDI}, \quad (4)$$

V^{loc} is the Skyrme force whereas V^{Coul} , V^{Yuk} and V^{MDI} define, respectively, the Coulomb, Yukawa and momentum dependent potentials. Yukawa term separates surface which also play role in low energy process like fusion and cluster radioactivity [13,14]. The momentum-dependent part of the interaction acts strongly in the cases where the system is mildly excited [15,16]. In this case, the MDI is reported to generate a lot more fragments compared to the static equation of state. For a detailed discussion of the different equations of state and MDI, the reader is referred to Refs. [4,15,16]. The relativistic effect does not play role in low incident energy of present interest.

The phase space of the nucleons is stored at several time steps. The QMD model does not give any information about the fragments observed at the final stage of the reaction. In order to construct fragments from the present phase-space one needs the clusterization algorithms. We shall concentrate here on the MST and MSTB methods only.

2.2 Different clusterization methods

2.2.1 Minimum spanning tree (MST) method

The widely used clusterization algorithm is the Minimum Spanning Tree (MST) method [12]. In MST method, two nucleons are allowed to share the same fragment if their centroids are closer than a distance r_{min} ,

$$|\mathbf{r}_i - \mathbf{r}_j| \leq r_{min}. \quad (5)$$

where \mathbf{r}_i and \mathbf{r}_j are the spatial positions of both nucleons. The value of r_{min} can vary between 2-4 fm. This method cannot address the question of time scale. This method gives a big fragment at high density which splits into several light and medium mass fragments after several hundred fm/c. This procedure gives same fragment pattern for times later than 200 fm/c, but cannot be used for earlier times.

2.2.2 Minimum spanning tree method with binding energy check (MSTB)

This is an improved version of normal MST method. Firstly, the simulated phase-space is analyzed with MST method and pre-clusters are sorted out. Each of the pre-clusters is then subjected to binding energy check [11]:

$$\zeta_i = \frac{1}{N^f} \sum_{i=1}^{N^f} \left[\frac{(\mathbf{p}_i - P_{N^f}^{cm})^2}{2m_i} + \frac{1}{2} \sum_{j \neq i}^{N^f} V_{ij}(\mathbf{r}_i, \mathbf{r}_j) \right] < E_{bind}. \quad (6)$$

We take $E_{bind} = -4.0$ MeV if $N^f \geq 3$ and $E_{bind} = 0.0$ otherwise. Here N^f is the number of nucleons in a fragment and $P_{N^f}^{cm}$ is center-of-mass momentum of the fragment. This is known as Minimum Spanning Tree method with Binding energy check (MSTB) [11]. The fragments formed with the MSTB method are reliable and stable at early stages of the reactions.

3 Results and Discussion

We have simulated the central reactions of $^{20}\text{Ne}+^{20}\text{Ne}$ ($E_{lab} = 10\text{-}55$ AMeV), $^{40}\text{Ar}+^{45}\text{Sc}$ ($E_{lab} = 35\text{-}125$ AMeV), $^{58}\text{Ni}+^{58}\text{Ni}$ ($E_{lab} = 35\text{-}105$ AMeV), $^{86}\text{Kr}+^{93}\text{Nb}$ ($E_{lab} = 35\text{-}95$ AMeV), $^{129}\text{Xe}+^{118}\text{Sn}$ ($E_{lab} = 45\text{-}140$ AMeV), $^{86}\text{Kr}+^{197}\text{Au}$ ($E_{lab} = 35\text{-}400$ AMeV) and $^{197}\text{Au}+^{197}\text{Au}$ ($E_{lab} = 70\text{-}130$ AMeV). The energies are guided by experiments [5–7]. For

the present study, we use hard (labeled as Hard), soft (Soft), Hard with MDI (HMD) and Soft with MDI (SMD) equation of state. We also use standard energy-dependent Cugnon cross section (σ_{nn}^{free}) [16] and constant isotropic cross section of 55 mb strength in addition to two different widths of Gaussian $L = 1.08$ and 2.16 fm^2 (L^{broad}). The superscript to the labels represent cross section. The phase-space is clusterized using clusterization methods described previously. The reactions are followed till 200 fm/c but the conclusions do not change when the reaction is over employing the validity of both algorithms.

In fig. 1, we display the time evolution of IMFs for the reaction $^{86}\text{Kr}+^{93}\text{Nb}$ at incident energy of 75 AMeV employing MST method. In fig. 1(a), we display the model calculations using Hard^{cug} (solid line) and Soft^{cug} (dashed line). From fig. 1(a), we see that the number of IMFs are larger in case of Soft as compared to Hard. This is because of the fact that soft matter will be easily compressed as a result of which density achieved will be more which in turn will lead to the large number of IMFs as compared to that in case of Hard. It is worth mentioning here that the effect could be opposite at higher energies. Since at higher energies the IMFs may further break into LCPs and free nucleons. In fig. 1(b), we display the results for Hard^{cug} and Hard^{55} (dotted line). As evident from the fig. 1(b), the number of IMFs are nearly same for both type of cross sections. This may be due to the fact that for the central collisions, since the excitation energy is already high therefore, different cross sections have a negligible role to play. In fig. 1(c), we display the results for Hard along with two different widths of Gaussian i.e. L and L^{broad} (dash-dotted line). We find that the width of Gaussian has a considerable impact on fragmentation. As we change the Gaussian width (L) from 4.33 to 8.66 fm^2 , the multiplicity of IMFs is reduced by $\approx 30\%$. Interestingly, the kaon yield also get reduced by the same amount

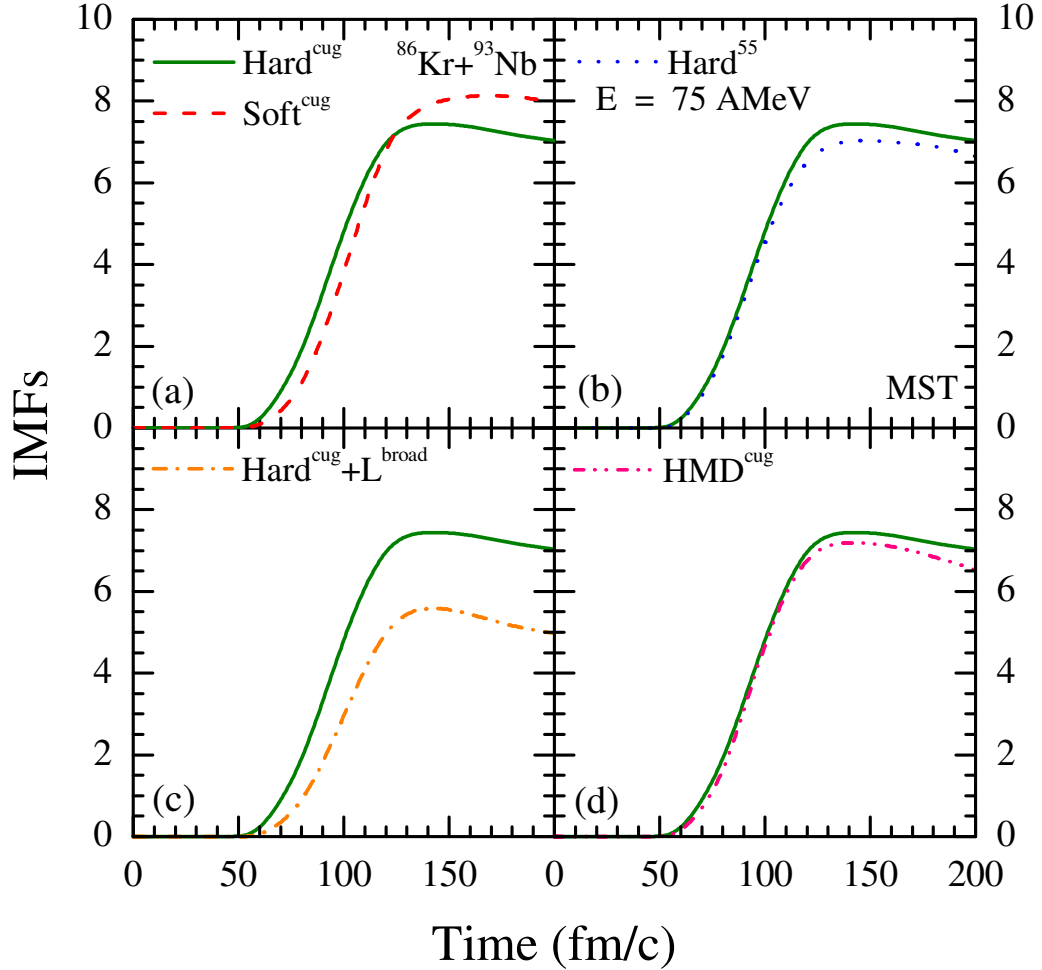


Figure 1: The time evolution of IMFs ($5 \leq A \leq 44$) for the reaction of $^{86}\text{Kr} + ^{93}\text{Nb}$ at incident energy of 75 A MeV for different model ingredients .

[17]. Due to its large interaction range, an extended wave packet (i.e. L^{broad}) will connect a large number of nucleons in a fragment, as a result it will generate heavier fragments as compared to one obtains with smaller width. It is worth mentioning here that the width of Gaussian has a considerable effect on the collective flow [17, 18] as well as pion production also [17, 19]. In fig. 1(d), we display the results using Hard and HMD (dash-dot-dot line). Again the number of IMFs are nearly same for both EOS. This is expected since

the effect of MDI will be small at these energies. However, the scenario is completely different at high energies. Since at high energies, due to the repulsive nature of MDI, there is large destruction of initial correlations and the additional momentum dependence further destroys the correlations reducing further the multiplicity of IMFs. This leads to the emission of lots of nucleons and LCPs [20].

In fig. 2, we display the average multiplicity of IMFs, $\langle N_{IMF} \rangle$, as a function of incident energy in the center-of-mass frame ($E_{c.m.}$) for $^{58}\text{Ni}+^{58}\text{Ni}$ reaction employing MST (open symbols) and MSTB (solid symbols) methods. Figs. 2(a) and 2(b) are for Soft^{cug} and Hard^{cug} , respectively. Lines represent the quadratic fit to the model calculations. In both cases, the number of IMFs first increases with incident energy, attains a maxima and then decreases in agreement with the previous studies [5–7, 10, 11]. Clearly, $\langle N_{IMF} \rangle$ is more for MST method as compared to MSTB method. Since in case of MSTB method along with spatial correlations, an additional check for binding energy is also used, therefore it filters out the loosely bound fragments which will decay later. Hence, the fragments obtained with MSTB method are properly bound. A similar trend is obtained for all other reactions as well as different model ingredients used in the present study but is less pronounced in lighter systems like $^{20}\text{Ne}+^{20}\text{Ne}$, $^{40}\text{Ar}+^{45}\text{Sc}$ as compared to heavier systems. However for Gaussian width L^{broad} , the $\langle N_{IMF} \rangle$ is nearly zero in this incident energy range using MSTB method (not shown here). This is due to the fact that an extended wave packet (i.e. L^{broad}) connects a large number of nucleons in a fragment, as a result it generates heavier fragments and the additional binding energy check further excludes the unbound fragments.

In fig. 3, we display the peak center-of-mass energy $E_{c.m.}^{max}$ as a function of combined

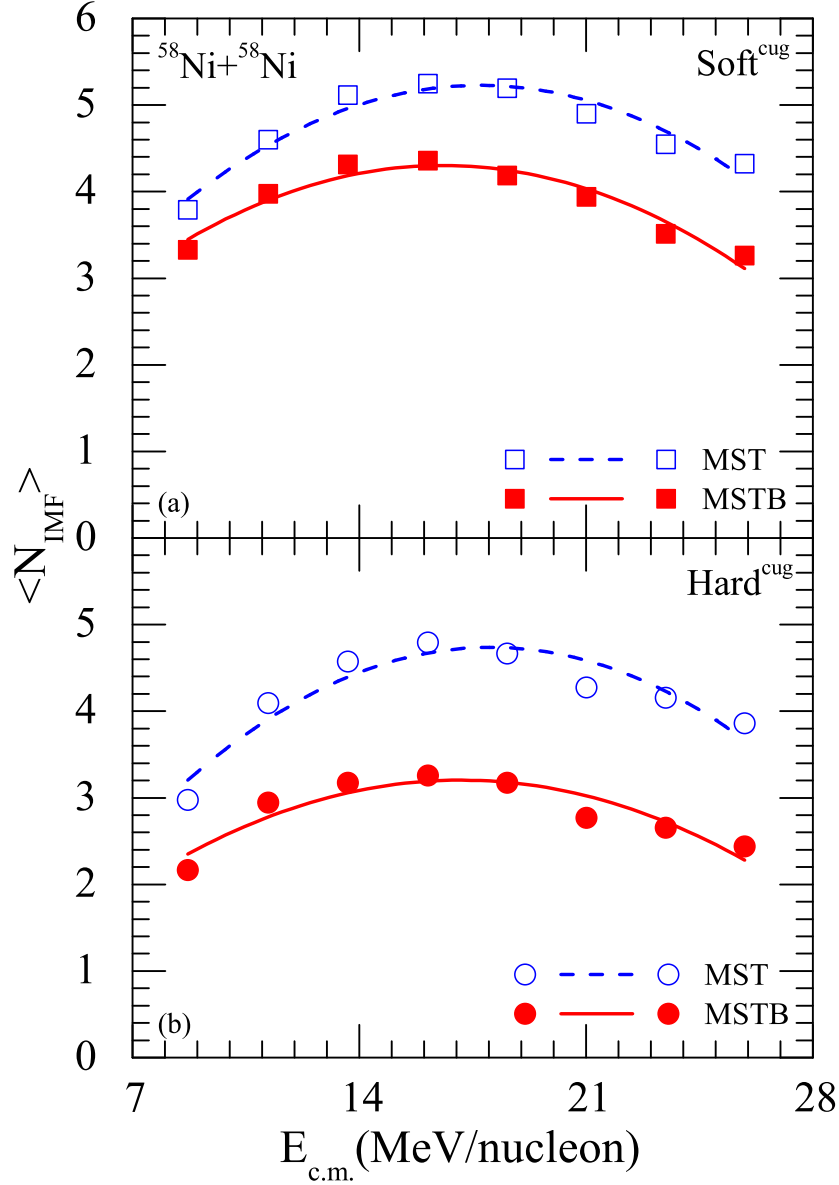


Figure 2: The mean IMF multiplicity, $\langle N_{IMF} \rangle$, as a function of incident energy in center-of-mass frame, $E_{c.m.}$, for the reaction of $^{58}\text{Ni} + ^{58}\text{Ni}$. Solid (dashed) curves show the quadratic fits to the model calculations for MSTB (MST) method to estimate the peak center-of-mass energy at which the maximal IMF emission occurs.

mass of the system employing MST method. Lines represent linear fitting proportional to mA . We find that the mass dependence of $E_{c.m.}^{max}$ is insensitive to different EOS (fig.

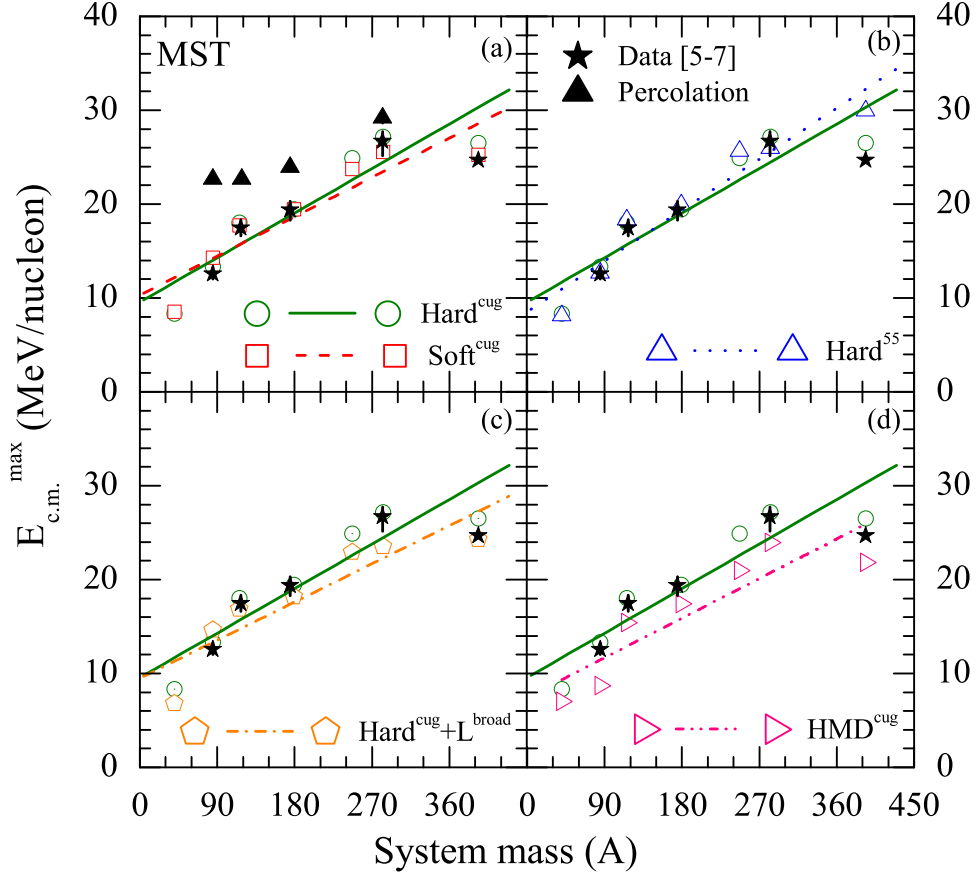


Figure 3: The $E_{c.m.}^{max}$ as a function of composite mass of the system (A). The different lines represent the linear fits. Comparison of model calculations is made with experimental data [5–7] (solid stars). The percolation calculations [6] (solid triangles) are also shown in figure.

3a), nn cross section (fig. 3b) as well as the width of Gaussian also (fig. 3c). It is slightly sensitive to MDI because for heavy systems $E_{c.m.}^{max}$ is more as a result of which the effect of MDI becomes non-negligible. In fig. 3, the model calculations are also compared with experimental data [5–7]. It is clear from the fig. 3 that model calculations for $E_{c.m.}^{max}$ agree with experimental data [5–7]. This behavior is consistent for all the different choices of

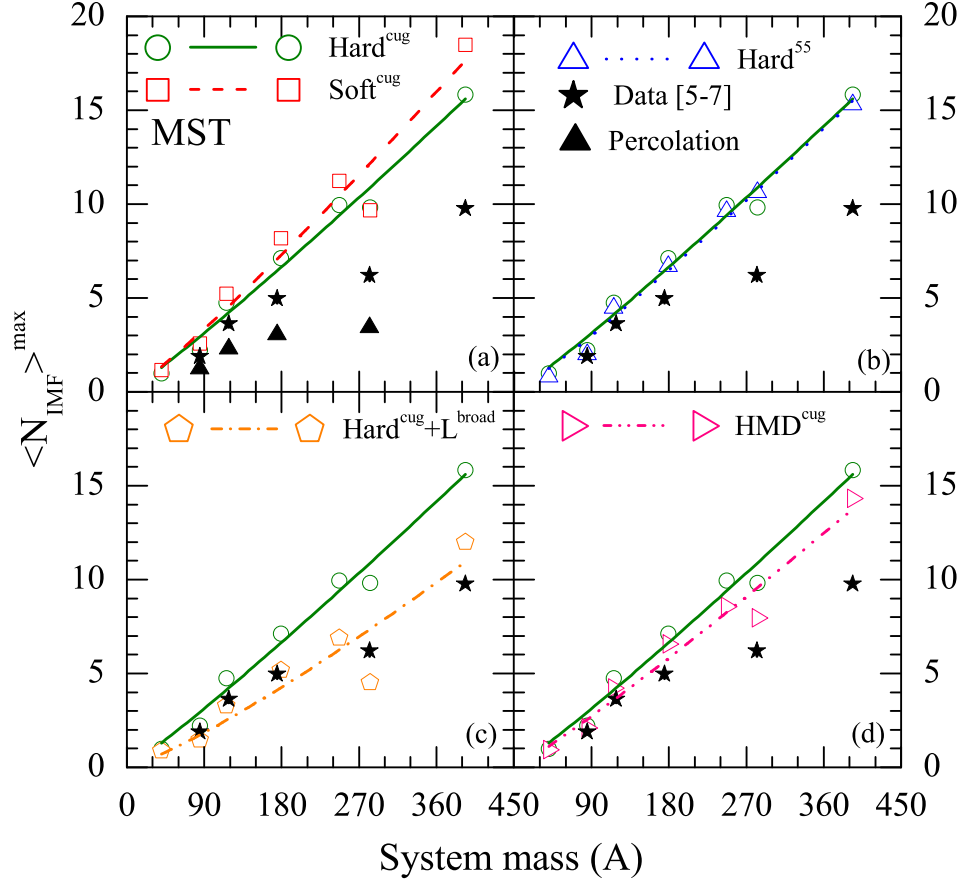


Figure 4: $\langle N_{IMF} \rangle^{max}$ as a function of composite mass of the system (A). The different lines represent the power law fits ($\propto A^\tau$). Comparison of model calculations is made with experimental data [5–7] (solid stars). The percolation calculations [6] (solid triangles) are also shown in figure.

model ingredients.

In fig. 4, we display the peak multiplicity of IMF fragments $\langle N_{IMF} \rangle^{max}$ as a function of combined mass of the system employing MST method. The lines represent power law fitting proportional to A^τ . The multiplicity of IMF fragments, in case of $^{20}\text{Ne}+^{20}\text{Ne}$ and $^{40}\text{Ar}+^{45}\text{Sc}$, is obtained by excluding the largest and second largest fragment, respectively, to get the ac-

curate information about the system size dependence. $\langle N_{IMF} \rangle^{max}$ are obtained by making a quadratic fit to the model calculations for $\langle N_{IMF} \rangle$ as a function of $(E_{c.m.})$. We find that the peak multiplicity is insensitive to cross section (fig. 4b) and MDI (fig. 4d) (for explanation see discussion of fig. 1). It is slightly sensitive to EOS (fig. 4a) but highly sensitive to the Gaussian width (fig. 4c). On increasing the width of Gaussian, $\langle N_{IMF} \rangle^{max}$ reduces to a large extent. As discussed earlier, an extended wave packet (i.e. L^{broad}) will connect a large number of nucleons in a fragment, as a result it generates heavier fragments as compared to one obtains with smaller width. From fig. 3, we see that $E_{c.m.}^{max}$ shows linear dependence ($\propto mA$) whereas $\langle N_{IMF} \rangle^{max}$ (fig. 4) follows power law behaviour ($\propto A^\tau$) with τ nearly equal to unity. In fig. 4, the model calculations are also compared with experimental data [5–7]. It is clear from the fig. 4 that, as the system mass increases difference between model calculations and experimental results goes on increasing. This behavior is consistent for all the different choices of model ingredients. This may be due to the fact that the fragments obtained with MST method are not reliable because this method makes sense only when matter is diluted and well separated. This is true only in case of high beam energy and in central collisions. Therefore, we have to look for other methods of clusterization. As mentioned earlier, the fragments obtained with MSTB method are properly bound and reliable. So, as a next step, we check system size dependence of $E_{c.m.}^{max}$ and $\langle N_{IMF} \rangle^{max}$ by using MSTB method for clusterization.

In fig. 5, we display the $E_{c.m.}^{max}$ (left panels) and $\langle N_{IMF} \rangle^{max}$ (right panels) for Soft^{cug} (upper panels) and Hard^{cug} (bottom panels) as a function of combined mass of the system. Solid (open) symbols represent MSTB (MST) method. From left panels we find that $E_{c.m.}^{max}$ remains insensitive to the choice of clusterization method. The same is true for

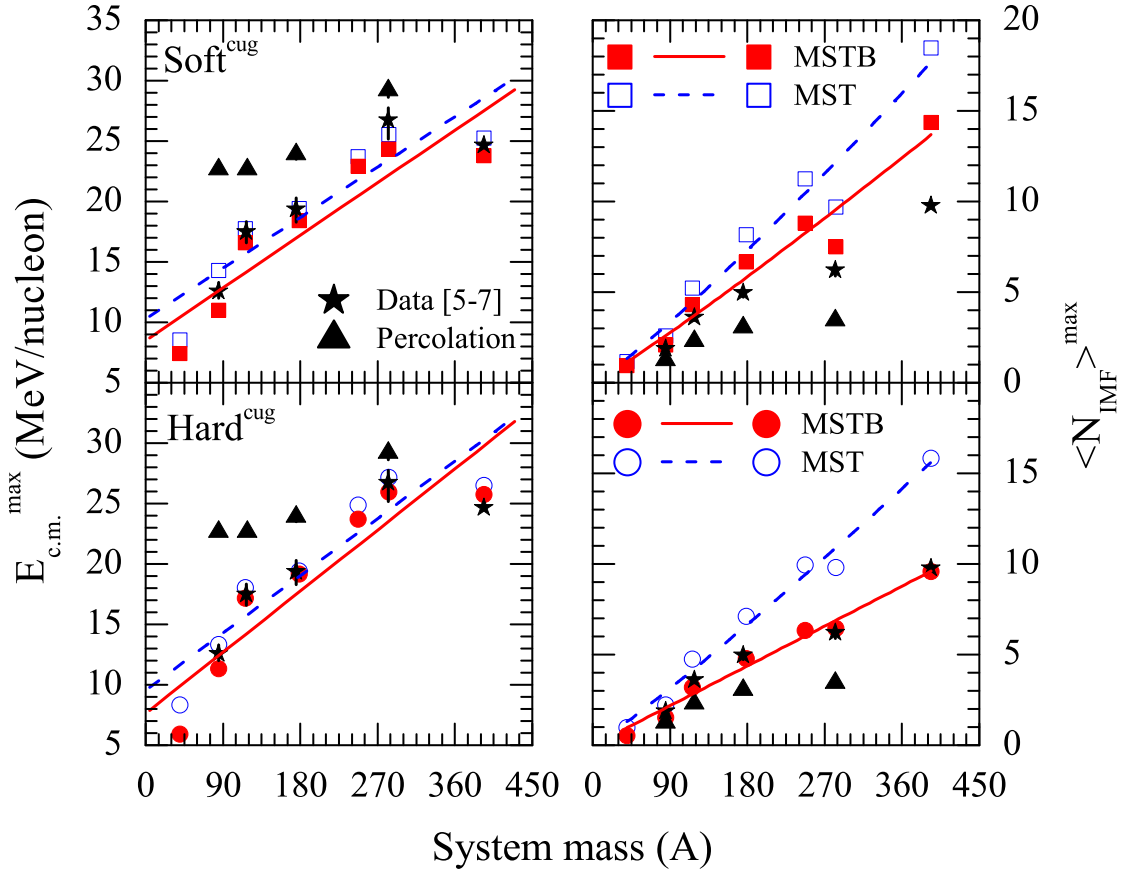


Figure 5: The $E_{c.m.}^{max}$ (left panels) and $\langle N_{IMF} \rangle^{max}$ (right panels) as a function of composite mass of the system (A) using Soft^{cug} (upper panels) and Hard^{cug} (lower panels) employing MSTB and MST methods. The different lines in left (right) panels represent the linear fits (power law fits). Comparison of model calculations is made with experimental data [5–7] (solid stars).

$\langle N_{IMF} \rangle^{max}$ (right panels) but in low mass region. As the system mass increases, the $\langle N_{IMF} \rangle^{max}$ becomes more and more sensitive to the method of clusterization. The MSTB method excludes the loosely bound fragments thus reducing the peak IMF multiplicity. The effect is uniform for both the EOS as well as for different cross section (not shown

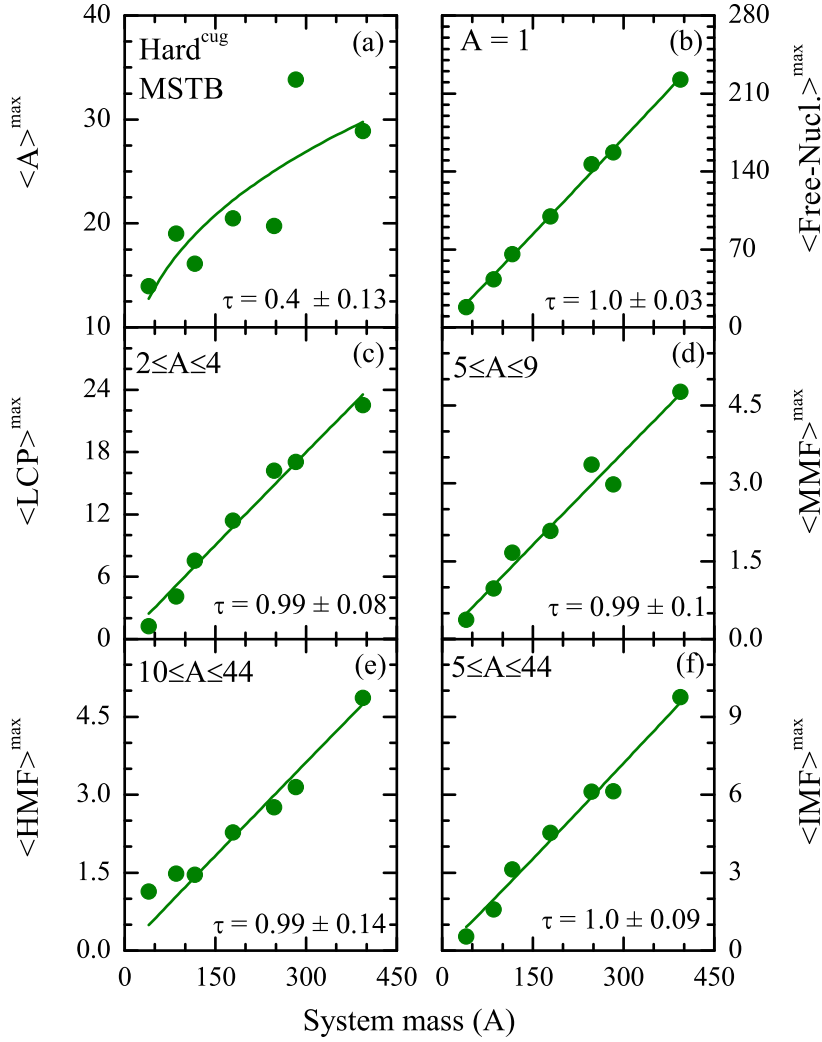


Figure 6: The largest fragment and multiplicities of free-nucleons, LCPs, MMFs, HMFs, and IMFs as a function of composite mass of the colliding nuclei (A) for different reactions at their respective $E_{c.m.}^{max}$ (solid circles). Lines represent the power law fits ($\propto A^\tau$).

here).

In fig. 6, we display peak multiplicity (obtained by employing MSTB method) as a function of composite mass of the system for various fragments consisting of the largest fragment (A^{max}) (fig. 6a), free-nucleons ($1 \le A \le 1$) (fig. 6b), light charged particles (LCPs) ($2 \le A \le 4$) (fig. 6c), medium mass fragments (MMFs) ($5 \le A \le 9$) (fig. 6d), heavy

mass fragments (HMFs) ($10 \leq A \leq 44$) (fig. 6e) and intermediate mass fragments (IMFs) ($5 \leq A \leq 44$) (fig. 6f) for Hard^{cug} . Lines represent the power law fitting proportional to A^τ . Interestingly, the peak multiplicities of different fragments follow a power law ($\propto A^\tau$). Power law factor τ is almost unity in all cases except A^{max} for which there is no clear system size dependence. The system size dependence of various fragments has also been predicted by Dhawan and Puri [21]. Their calculations at the energy of vanishing flow (i.e., the energy at which the transverse flow vanishes) clearly suggested the existence of a power law system mass dependence for various fragment multiplicities.

4 Summary

We have simulated the central reactions of nearly symmetric, and asymmetric systems over the entire periodic table at different incident energies for the different equations of state (EOS), nn cross sections and different widths of Gaussians. We have observed that the multiplicity of intermediate mass fragments (IMFs) ($3 \leq Z \leq 20$) shows a rise and fall with increase in beam energy in the center-of-mass frame as already predicted experimentally/theoretically. We have also studied the system size dependence of peak center-of-mass energy $E_{c.m.}^{max}$ and peak IMF multiplicity $\langle N_{IMF} \rangle^{max}$. It has been observed that $E_{c.m.}^{max}$ increases linearly with system mass whereas a power law ($\propto A^\tau$) dependence has been observed for $\langle N_{IMF} \rangle^{max}$ with $\tau \sim 1.0$. We have compared system size dependence of $E_{c.m.}^{max}$ and $\langle N_{IMF} \rangle^{max}$ for MST and MSTB methods and found that MSTB method reduces the $\langle N_{IMF} \rangle^{max}$ especially in heavy systems because in MSTB method due to binding energy check loosely bound fragments get excluded. The power law dependence

is also observed for fragments of different sizes at the energy for which the production of IMFs is maximum and power law parameter τ is found to be close to unity in all cases except A^{max} .

5 Acknowledgements

This work has been supported by a grant from Department of Science and Technology (DST), Government of India, India.

References

- [1] R. K. Puri, C. Hartnack, and J. Aichelin, Phys. Rev. C **54**, R28 (1996); *ibid.*, J. Comput. Phys. **162**, 245 (2000); Y. K. Vermani and R. K. Puri, Europhys. Lett. **85**, 62001 (2009); *ibid.*, J. Phys. G: Nucl. Part. Phys. **37**, 015105 (2010); S. Kumar, S. Kumar, and R. K. Puri, Phys. Rev. C **78**, 064602 (2008).
- [2] S. Kumar, M. K. Sharma, and R. K. Puri, Phys. Rev. C **58**, 3494 (1998); A. D. Sood *et al.*, Phys. Rev. C **79**, 064618 (2009); *ibid.*, Phys. Rev. C **70**, 034611 (2004); S. Kumar, S. Kumar, and R. K. Puri, Phys. Rev. C **81**, 014611 (2010); S. Kumar *et al.*, Phys. Rev. C **81**, 014601 (2010); E. Lehmann *et al.*, Prog. Part. Nucl. Phys. **30**, 219 (1993); *ibid.*, Phys. Rev. C **51**, 2113 (1995).
- [3] J. Singh, S. Kumar, and R. K. Puri, Phys. Rev. C **62**, 044617 (2000); G. Batko *et al.*, J. Phys. G: Nucl. Part. Phys. **20**, 461 (1994); S. W. Huang *et al.*, Prog. Part.

- Nucl. Phys. **30**, 105 (1993); R. K. Puri *et al.*, Nucl. Phys. A **575**, 733 (1994); C. Fuchs *et al.*, J. Phys. G: Nucl. Part. Phys. **22**, 131 (1996).
- [4] M. Begemann-Blaich *et al.*, Phys. Rev. C **48**, 610 (1993); D. R. Bowman *et al.*, Phys. Rev. Lett. **67**, 1527 (1991); A. Schuttauf *et al.*, Nucl. Phys. A **607**, 457 (1996); W. Reisdorf *et al.*, Nucl. Phys. A **612**, 493 (1997).
- [5] M. B. Tsang *et al.*, Phys. Rev. Lett. **71**, 1502 (1993).
- [6] D. Sisan *et al.*, Phys. Rev. C **63**, 027602 (2001).
- [7] G. F. Peaslee *et al.*, Phys. Rev. C **49**, R2271 (1994).
- [8] R. T. de Souza *et al.*, Phys. Lett. B **268**, 6 (1991).
- [9] N. T. B. Stone *et al.*, Phys. Rev. Lett. **78**, 2084 (1997).
- [10] C. A. Ogilvie *et al.*, Phys. Rev. Lett. **67**, 1214 (1991).
- [11] Y. K. Vermani and R. K. Puri, J. Phys. G: Nucl. Part. Phys. **36**, 105103 (2009).
- [12] J. Aichelin, Phys. Rep. **202**, 233 (1991).
- [13] R. K. Puri and R. K. Gupta, Phys. Rev. C **45**, 1837 (1992); *ibid.*, Eur. Phys. J A **3**, 277 (1998); *ibid.*, Phys. Rev. C **43**, 315 (1991); *ibid.*, Eur. Phys. J A **8**, 103 (2000); I. Dutt and R. K. Puri, Phys. Rev. C **81**, 047601 (2010); *ibid.* C **81**, 044615 (2010); *ibid.* C **81**, 064609 (2010); *ibid.* C **81**, 064608 (2010); R. K. Puri and N. K. Dhiman, Eur. Phys. J A **23**, 429 (2005).
- [14] S. S. Malik *et al.*, Pram. J. Phys. **32**, 419 (1989); R. K. Puri and R. K. Gupta, J. Phys. G: Nucl. Part. Phys. **18**, 903 (1992).

- [15] S. Goyal, Phys. Rev. C **83**, 047601 (2011); *ibid.*, Nucl. Phys. A. **853**, 164 (2011).
- [16] S. Kumar, R. K. Puri, and J. Aichelin, Phys. Rev. C **58**, 1618 (1998); V. Kaur *et al.* Phys. Lett. B **697**, 512 (2011).
- [17] C. Hartnack *et al.*, Eur. Phys. J A **1**, 151 (1998).
- [18] S. Gautam *et al.*, J. Phys. G: Nucl. Part. Phys. **37**, 085102 (2010); S. Gautam and A. D. Sood, Phys. Rev. C **83**, 014603 (2011); *ibid.*, C **83**, 034606 (2011); A. D. Sood *et al.*, Phys. Rev. C **69**, 054612 (2004); *ibid.* C **73**, 067602 (2006); *ibid.*, Eur. Phys. J. A **30**, 571 (2006).
- [19] C. Hartnack *et al.*, Nucl. Phys. A **580**, 643 (1994).
- [20] Y. K. Vermani, S. Goyal, and R. K. Puri, Phys. Rev. C **79**, 064613 (2009).
- [21] J. K. Dhawan and R. K. Puri, Phys. Rev. C **74**, 054610 (2006).